Pathways of marine debris derived from trajectories of Lagrangian drifters

Nikolai Maximenko [a,*], Jan Hafner [a], Peter Niiler [b]

[a] International Pacific Research Center, School of Ocean and Earth Science and Technology, University of Hawaii, Honolulu, HI, United States
[b] Scripps Institution of Oceanography, University of California, San Diego, La Jolla, CA, United States

ARTICLE INFO

ABSTRACT

Global set of trajectories of satellite-tracked Lagrangian drifters is used to study the dynamics of marine debris. A probabilistic model is developed to eliminate the bias in spatial distribution of drifter data due to heterogeneous deployments. Model experiments, simulating long-term evolution of initially homogeneous drifter array, reveal five main sites of drifter aggregation, located in the subtropics and maintained by converging Ekman currents. The paper characterizes the geography and structure of the collection regions and discusses factors that determine their dynamics. A new scale $R_c = (4k/|D|)^{1/2}$ is introduced to characterize tracer distribution under competing effects of horizontal divergence D and diffusion k. Existence and locations of all five accumulation zones have been recently confirmed by direct measurements of microplastic at the sea surface.

© 2011 Elsevier Ltd. All rights reserved.

1. Introduction

The problem of marine debris became recently well recognized by the society.[1] As a kind of man-made pollution, debris does not only threaten the safety of maritime but also the health of the ecosystem. Local solutions of the problem are complicated by the ability of the debris to travel over large distances, carried by ocean current. Dynamics of the upper ocean and its mixed layer, where much of marine debris floats, is tremendously complex. While charts of surface currents existed since the times of first sails, even 20 years ago their accuracy was questionable. The datasets based on the ship drift provided, probably, the most adequate description of surface currents for that time. Wakata and Sugimori (1990) used the velocities gridded by Meehl (1982) on a 5-degree grid for four seasons to simulate trajectories of floating particles and to identify the areas, where the particles tend to collect in different seasons. They found large number of sites with the elevated number of model particles, each having size from a few hundred to 1000 km, rarely persisting throughout all the seasons. While some sites of debris accumulation, suggested by Wakata and Sugimori (1990), agreed with the observations, existing at that time, general patterns were noisy because of the low quality of the ship drift data. To understand the dynamics of debris in the North Pacific, Kubota (1994) performed simulations using a simple model, combining climatological estimates of geostrophic, Ekman, and Stokes currents. In his model, floating matter is first collected by Ekman currents on the northern flank of trade winds, then advected eastward by geostrophic currents, and finally kept north of the Hawaiian Islands. Later, using satellite data of geostrophic currents and winds, Kubota et al. (2005) improved the model, so that the final destination of debris shifted to northeast of Hawaii and is close to the location of now-famous Great Pacific Garbage Patch. Kubota et al. (2005) showed that in their model the same mechanism works in other four subtropical oceans. Martinez et al. (2009) performed similar modeling (but at higher spatial resolution and using time-varying currents) and concluded that the same mechanism, as described by Kubota (1994) in the North Pacific, collects floating marine debris in the eastern part of the subtropical South Pacific. In all these studies, Ekman currents, responsible for the existence of surface convergences were estimated using very simplistic models implying constant viscosity, an assumption, contradicting to modern observations (e.g., Ralph and Niiler, 1999) and models of the mixed layer.

In this paper, for the first time, to study the pathways of marine debris, we use the global set of historical trajectories of drifting buoys deployed in the Surface Velocity Program and Global Drifter Program to measure surface currents. We also compare between two designs of the drifters (drogued and undrogued) to prove the robustness of the conclusions of this study on the basin scale.

2. Drifter dataset

Utilized in this work are the trajectories of 10,561 drifters released during the Surface Velocity Program (SVP) that later developed into the Global Drifter Program (GDP). This network of drifting buoys provided a unique dataset (Niiler, 2001) spanning the period from February 15, 1979 through January 1, 2007. Each

* Corresponding author.
  E-mail addresses: maximenk@hawaii.edu (N. Maximenko), jhafner@hawaii.edu (J. Hafner), pniiler@ucsd.edu (P. Niiler).
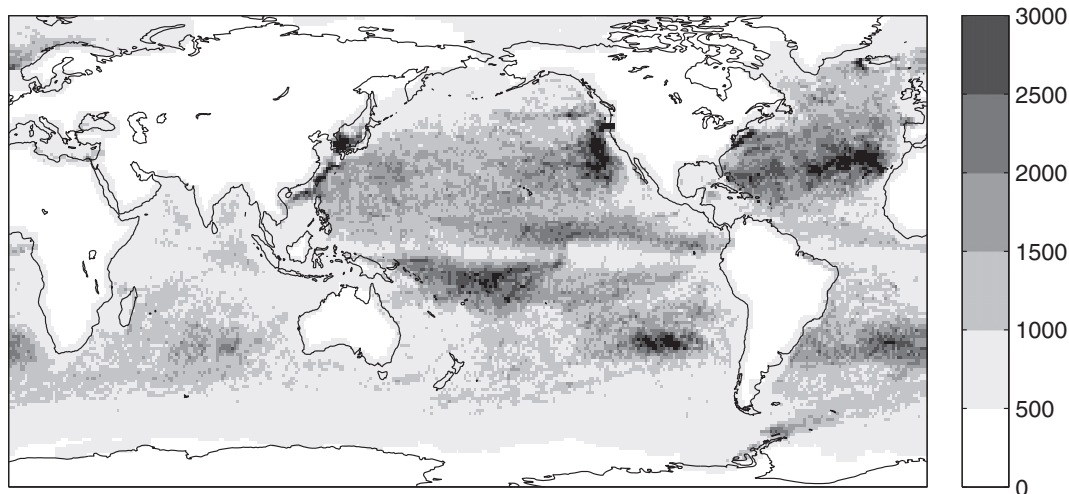 [1] www.5imdc.org

Fig. 1. Number of 6-hourly drifter data in 1-degree bins.

drifter is initially comprised of a large 'holey-sock' drogue, attached to the surface float, containing the transmitter, whose coordinates are detected by the satellite system ARGOS (Sybrandy and Niiler, 1991). At calm sea, the drogue occupies the depth range between 12 and 18 m, and for physical applications drifter measurements are usually interpreted as the current velocity at 15 m (e.g., (Niiler and Paduan, 1995)). Niiler et al. (1987) used a simple theoretical model to assess the drifter response to the joint effect of vertically sheared ocean current and wind. In the presence of breaking wind waves and Langmuir circulation, actual dynamics of the drifter is by far more complex than models can describe. Yet, the unified design of the drifters allows statistical description of their motions even without full understanding of the underlying physics.

As a first step, data from the drifters with their drogues intact were combined with the data of drifters that lost their drogues. The quality-controlled data, optimally interpolated Hansen and Poulain, 1996] onto 6-hourly intervals, were acquired from the NOAA AOML.[2] Fig. 1 shows the spatial distribution of the data. High heterogeneity of the density of drifters is both due to their massive launch in a set of local experiments and the result of advection by ocean currents. Effects of these two factors are illustrated by Fig. 2, showing distributions of initial and final positions of drifters. Among other locations, drifters were deployed in large numbers off the California coast, north of the Cape Hatteras, in the Japan/East Sea, and west of the Gibraltar Strait. These experiments provided high density of drifter data in their study domains. Comparison between Fig. 2a and b reveals regions where effect of ocean currents on the drifter array is stronger than the effect of their initial deployment. For instance, a large number of drifters was deployed at or near the equator in the Pacific Ocean, but these buoys were quickly removed to higher latitudes by the strong wind-driven equatorial divergence, so that the total number of data is small along the equator in Fig. 1. Similarly, density is also low in many regions of coastal upwelling. On contrary, not many drifters were released in the five subtropical regions (Fig. 2b), but many more were collected there by converging currents. Three of these regions (North Atlantic and eastern North and South Pacific), together with two other areas in the South Atlantic and Indian oceans, where the effect of currents is not so distinct in the unprocessed dataset, will be discussed in this paper as the areas of potential aggregation of marine debris. To isolate the effect of the currents from the influence of initial

deployments, the technique has been developed as described in the next section.

3. Statistical model of drifter spread

A chance for a drifter to move from its initial position $\mathbf{r_0} = (x_0, y_0)$ at time t_0 to point $\mathbf{r} = (x, y)$ at time t can be characterized by the probability density function $P(\mathbf{r_0}, t_0|\mathbf{r}, t)$. Numerically, the size of the matrix $P(\mathbf{r_0}, t_0|\mathbf{r}, t)$ is enormous in the general case, when matrix is also very sparse because of the limited number of available drifter trajectories. For example, the current drifter array consists of only 1341 drifters or one drifter per a 5° bin. In addition, data coverage of different basins was varying in time significantly. To mitigate the problem, we assume that the process of the drifter spreading is statistically stationary. This means that the probability for a drifter to travel between two locations depends only on the duration of the travel but does not depend on the selection of the start time moment, or $P(\mathbf{r_0}, t_0|\mathbf{r}, t) = P(\mathbf{r_0}|\mathbf{r}; t - t_0)$. Further simplification can be achieved for the travel times T longer than the Lagrangian decorrelation time. In this case, drifter 'forgets' its history and statistical evolution of the drifter array over time $T \cdot n$ (where n is integer) can be derived in n iterations, each of duration T.

For numerical computations, P was gridded to represent the probability for a drifter to move between the bins of size $1/2°$ latitude by $1/2°$ longitude. The time step T was set equal to 5 days that is larger than the typical Lagrangian time scale of the North Atlantic eddy field (Lumpkin et al., 2002). Over this time, a drifter moving at the characteristic velocity of 10 cm/s travels over the distance close to the size of the bin. $P(\mathbf{r_0}|\mathbf{r}; T)$ was calculated from the number of drifter excursions $N(\mathbf{r_0}|\mathbf{r}; T)$ between the pairs of bins by processing all the pairs of 6-hourly fixes from the same drifter, separated by 5 days.

Probability for a drifter to move over time T from bin $\mathbf{r_0}$ to bin $\mathbf{r}$

$$P(\mathbf{r_0}|\mathbf{r}; T) = N(\mathbf{r_0}|\mathbf{r}; T) / \int N(\mathbf{r_0}|\mathbf{r}; T) \cdot d\mathbf{r}, \qquad (1)$$

and examples of distribution of non-zero elements of P are shown in Fig. 3 for every 20th $\mathbf{r_0}$ bin in longitude and every 10th in latitude. This probability function can now be used to calculate the evolution of the drifter density C over T = 5 days as

$$C(\mathbf{r}, t + T) = \int C(\mathbf{r_0}, t) \cdot P(\mathbf{r_0}|\mathbf{r}; T) \cdot d\mathbf{r_0} + S(\mathbf{r}), \qquad (2)$$
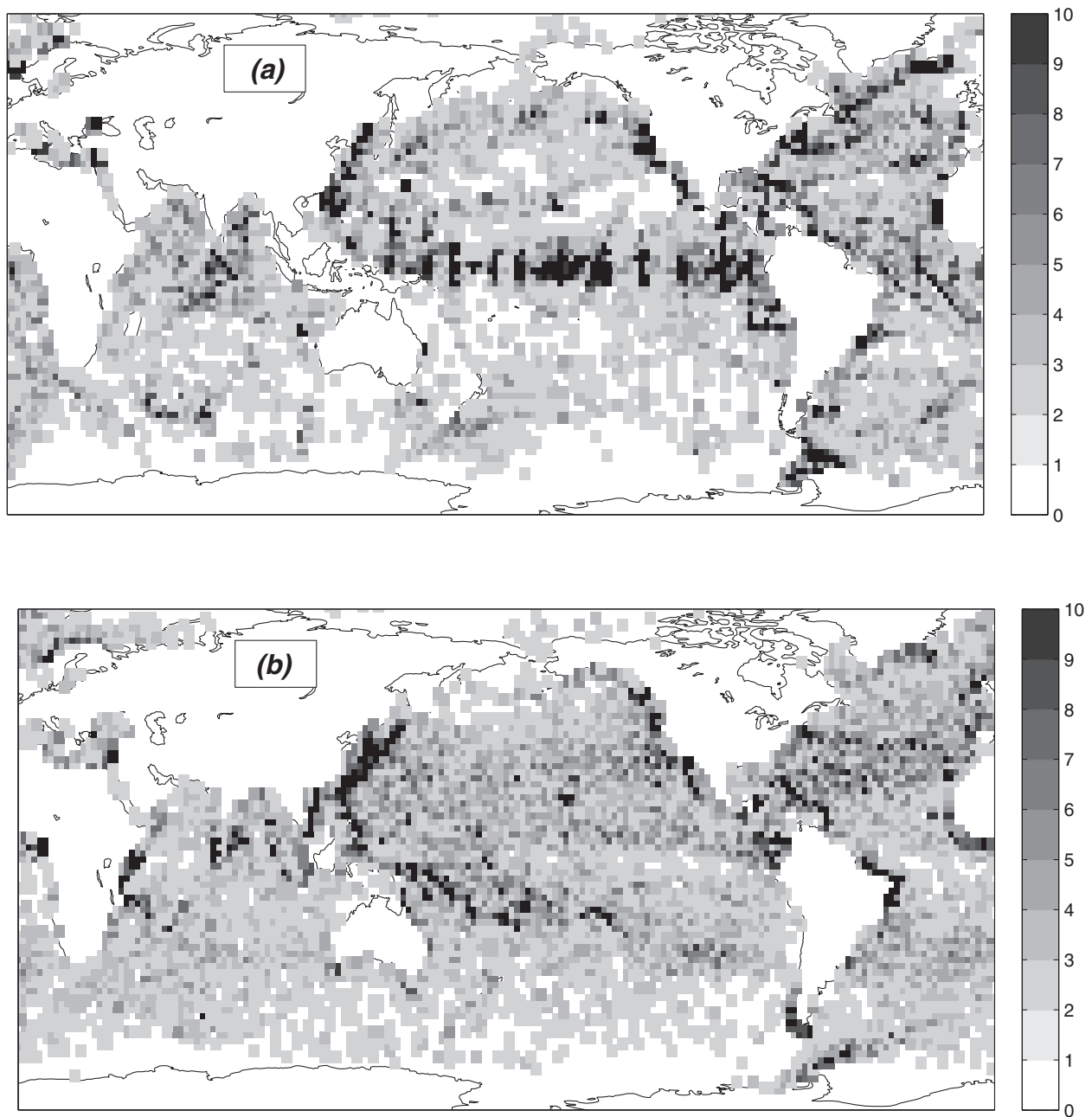
Fig. 2. Numbers of (a) start and (b) end points of drifters, used in this study, in 2-degree bins.

where S is the source of drifters and integration is over the bins with non-zero $C(\mathbf{r_0}, t)$. Used iteratively, Eq. (2) is the principal part of the model, used in this paper to simulate movement and spread of drifters under the effect of ocean currents from various initial states and sources.

4. Model experiment: drifter density evolution from homogeneous initial condition

As was discussed in previous sections, distribution of drifters in space depends not only on ocean currents but also on locations and intensity of drifter sources. In the case of marine debris, such sources are not well documented and understood. However, a simple model experiment can be carried out to detect locations of

main regions where floating matter accumulates on a long run. The experiment starts from the homogeneous initial condition $C = 1$ in all bins, where P is defined. Naturally, the bins, where P is not defined, are not included into the model. The bins, where at least one 5-day-long fragment of drifter trajectory ends up and no new fragments begin, serve as sinks of the tracer in the model. Such bins are commonly located along the coast, where drifters often end on the shore. As the model iterations, described by Eq. (2), continue, the solution 'forgets' the initial state and forms a pattern, from which regions of drifter aggregation can be identified. Maps of the solution, shown in Fig. 4,[3] indicate that drifters are quickly (in 1 year, Fig. 4b) washed away from the equatorial and coastal

---

[3] Tracking ocean debris//IPRC Climate, vol. 8. no. 2, p. 14–16.
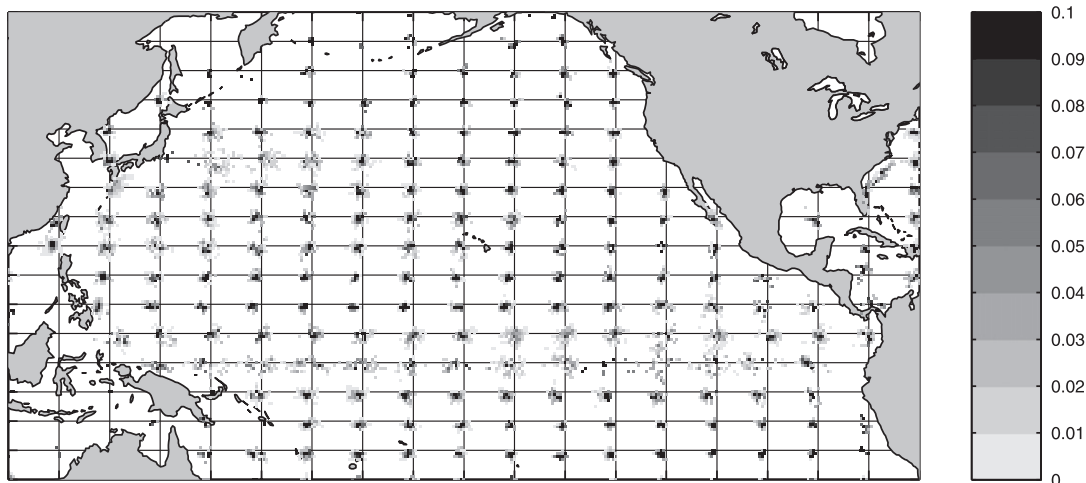
Fig. 3. Probability of drifter location in 1/2-degree bins after 5 days of travel from the near knot of the shown grid (10° longitude by 5° latitude).

areas, associated with strong wind-driven upwelling. In three years (Fig. 4c), tropical and subpolar regions are essentially cleared from the model drifters, most of which are pushed into the five subtropical gyres. In ten years (Fig. 4d), drifters are redistributed within and between the subtropical gyres to form more compact clusters, centered around 30° latitude. The North and South Pacific clusters are located in eastern parts of corresponding subtropical gyres, while the North and South Atlantic as well as the South Indian cluster are elongated zonally across the entire basins. The dissipation of the model solution in time is remarkably slow; 70% of the tracer remains in the ocean after 10 years of integration.

Location of the North Pacific cluster in Fig. 4d coincides with the location of the so-called Great Garbage Patch (*e.g.*, Moore et al., 2001). Location of the North Atlantic cluster is also consistent with the observations revealing high concentration of defragmented plastic (Law et al., 2010). To the authors' best knowledge, observations of marine plastic or any other kind of debris in the three other clusters, seen in Fig. 4d in the Southern Hemisphere, were completely missing until very recently. Evolution of the model solution in time is qualitatively consistent with the pattern of ensemble-mean currents, derived from drifter trajectories and shown in Fig. 5a. Model clusters in different oceans differ in size, shape, and strength, perhaps, because of the differences in mean currents and their variability.

The largest value of the model solution in Fig. 4d, found in the eastern South Pacific, is collocated with the center of the best pronounced swirling convergence in Fig. 5a. Although accumulation of defragmented plastic and other debris in this patch is yet to be verified, drifters from many sources do show the tendency to aggregate in relatively compact area of Fig. 6a. Figs. 1 and 2b also show a local data density maximum where only few trapped drifters were deployed initially (Fig. 2a). Fig. 6b illustrates that after entering the convergence area drifters remain there for the rest of their lives.

If currents were stationary, the process of debris collection in the ocean would be somewhat similar to rainwater collection on the land. A floating particle, released at given location, would be destined to move along one of streamlines, shown in Fig. 5a, until reaching its end either in one of the convergence centers or on the shore. Each center would be collecting drifters from a separate area. Fig. 5b illustrates the geographic distribution of such collection areas, having rather complex shapes. In addition, streamlines in Fig. 5a in 'yellow' areas of Fig. 5b are ending in secondary convergences, many of which are induced by the noise in the ensemble-averaged drifter velocities.

In reality, ocean currents are not steady but exhibit broad spectrum of variability, from inertial oscillations and tides to mesoscale eddies to seasonal, interannual and interdecadal variations. In the statistically stationary model, described in this section, this variability is present as diffusion, allowing a particle to move differently from the mean streamlines of Fig. 5a. This diffusion also allows the model drifters to escape from the convergence zones and causes the general decay of the model solution on the long run. Fig. 7 shows how maximum values of the model solution change in time in the five subtropical gyres. The concentration C increases from the unity to maximum values of 15, 15, 30, 45, and 150 in the South Indian, North and South Atlantic, and North and South Pacific patches, respectively, before it starts to decrease. Maximum values are not proportional to the collection areas in Fig. 5b that indicates that active drifter exchange between the patches takes place in the model. The maxima are reached after 6, 10, 25, 25, and 300 years of integration, respectively, that provides an estimate of the 'turn-around' time scale for the five convergent systems.

Time-varying surface currents or diffusion give the model drifters a liberty of taking plural paths that link virtually any two locations on the ocean map. Collection areas in this case can be characterized by sorting locations according to the minimum time, required to reach one of the five convergent centers, marked in Fig. 4d. The underlying idea here is that debris pathways favored by ocean currents are also the fastest routes between source and destination. This time can be also used to assess minimum age of debris of different origin in the patches. It can be easily computed by reversing the velocity fields from $\mathbf{V}(\mathbf{r}, \underline{t})$ to $-\mathbf{V}(\mathbf{r}, -t)$ and computing 'backward' trajectories, starting from the collection center A. In the statistical model, the probability of the reversed currents is described by

$$P_B(\mathbf{r_0}|\mathbf{r};T) = N(\mathbf{r_0}|\mathbf{r};T) \Big/ \int N(\mathbf{r_0}|\mathbf{r};T) \cdot d\mathbf{r_0} \qquad (3)$$

and solution of the reversed model is

$$C_B(\mathbf{r}, t+T) = \int C_B(\mathbf{r_0}, t) \cdot P_B(\mathbf{r_0}|\mathbf{r};T) \cdot d\mathbf{r_0} + S(\mathbf{r}_A) \qquad (4)$$

where integration is over the bins with non-zero $C_B(\mathbf{r_0}, t)$, and $S(\mathbf{r}_A)$ is the source at location A. At every point the time was recorded when the solution changed from its initial zero value. After repeating the model experiment for all five collection centers, the absolute minimum time is plotted in Fig. 8a and the index of the nearest (in terms of time needed to reach) center is shown in Fig. 8b.
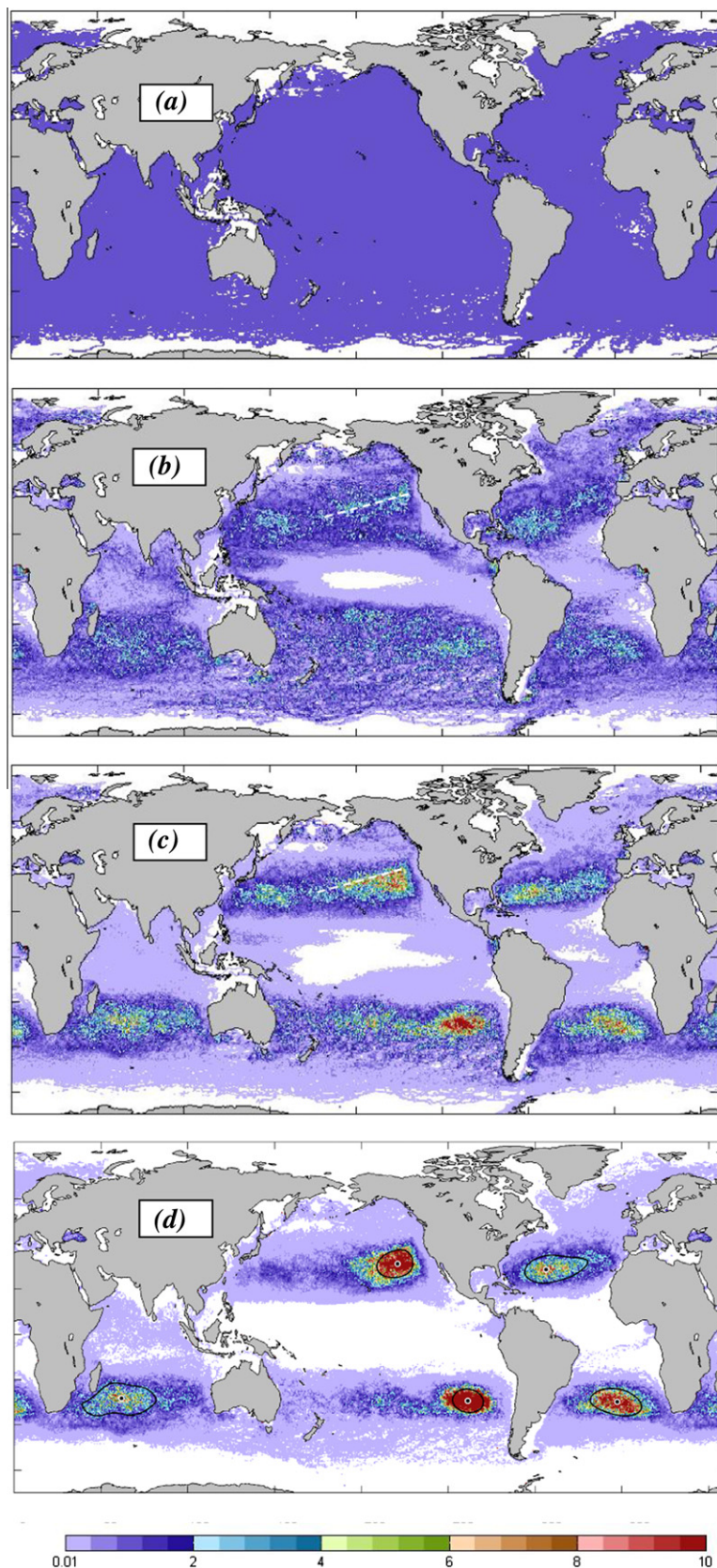
Fig. 4. Maps of the model solution C after (b) 1 year, (c) 3 years, and (d) 10 years of integration from the initially homogeneous state (a) $C = 1$. Dots in (d) mark positions of five subtropical maxima, and contours are isopleths, corresponding to halves of these maximum values, calculated after smoothing the solution with the two-dimensional Hanning filter with 1000 km half-width. White dashed lines in (b) and (c) denote the location of the North Pacific subtropical front. For (d) see also Dohan and Maximenko (2010) and Kershaw et al. (2011).
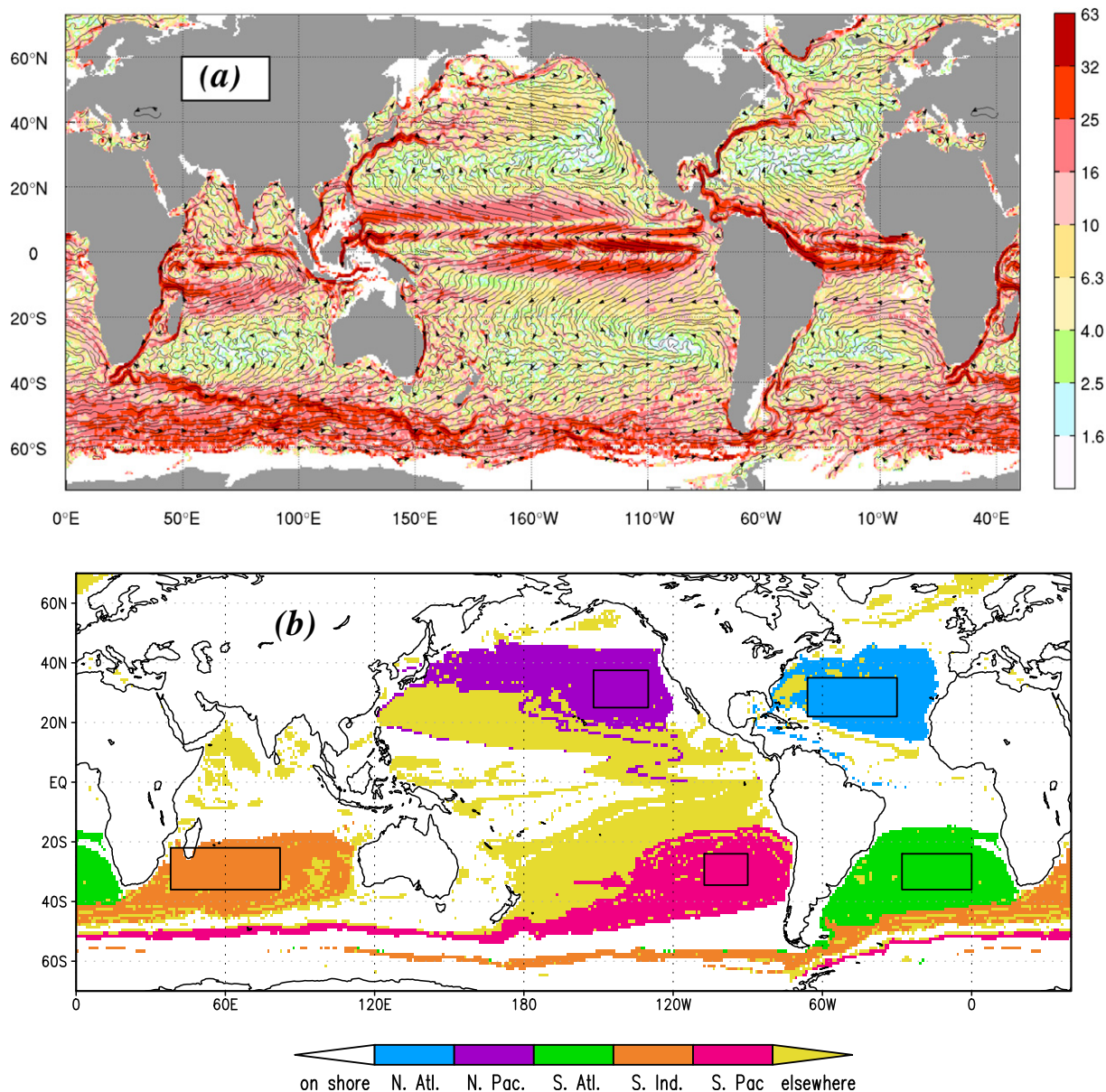
Fig. 5. (a) Ensemble-mean streamlines overlaid on velocity magnitude (colors), derived from drifter trajectories (Maximenko et al., 2009). (b) Areas, from which five zones collect particles, advected by the currents, shown in (a). Units in (a) on are cm/s. Colors in (b) indicate final destination within rectangles, built around contours of Fig. 4d.

Differences between Figs. 8a and 5a are tremendous and they illustrate the important role that temporal variability of currents plays in the fate of marine debris. In the excellent agreement with the model solution in Fig. 4, practically every part of the world ocean is linked in Figure 8a to at least one collection center. These connections also explain the lower (30%) loss of drifters by the diffuse model that estimated for the stationary currents (45%) from the fraction of white areas in Fig. 5b. Effect of the mean current is less pronounced in Fig. 8a (than in Fig. 5a) but is still clearly seen in many areas. For instance, time to reach the near center is reduced along axes of the eastward-flowing Gulf Stream and Kuroshio Extension and increased in the westward North Equatorial Current. The strong Antarctic Circumpolar Current dramatically slows-down or even arrests westward motions in the Southern Ocean, so that drifters, released in the Indian Ocean southwest of Australia, end up in the South Pacific collection center, and drifters, originating from the southeastern corner of the Pacific, end up in the South Atlantic.

It is important to note that Fig. 8 represents most extreme events, not the most probable dynamics. The latter would require much more sophisticated and time-consuming computations.

5. Summary and discussion

Trajectories of SVP/GDP drifters were used in this work to study the pathways of marine debris in the global upper ocean. A probabilistic model was developed to eliminate the bias existing due to the highly heterogeneous distribution of data in space. Possible impact of unknown distribution of sources of debris in the real ocean was mitigated by the model integration over long time periods.

The model solution reveals five main areas of the debris aggregation (Fig. 4d), all lying in the subtropics, centered approximately at 30° latitude. Locations of the North Pacific[4] and North Atlantic
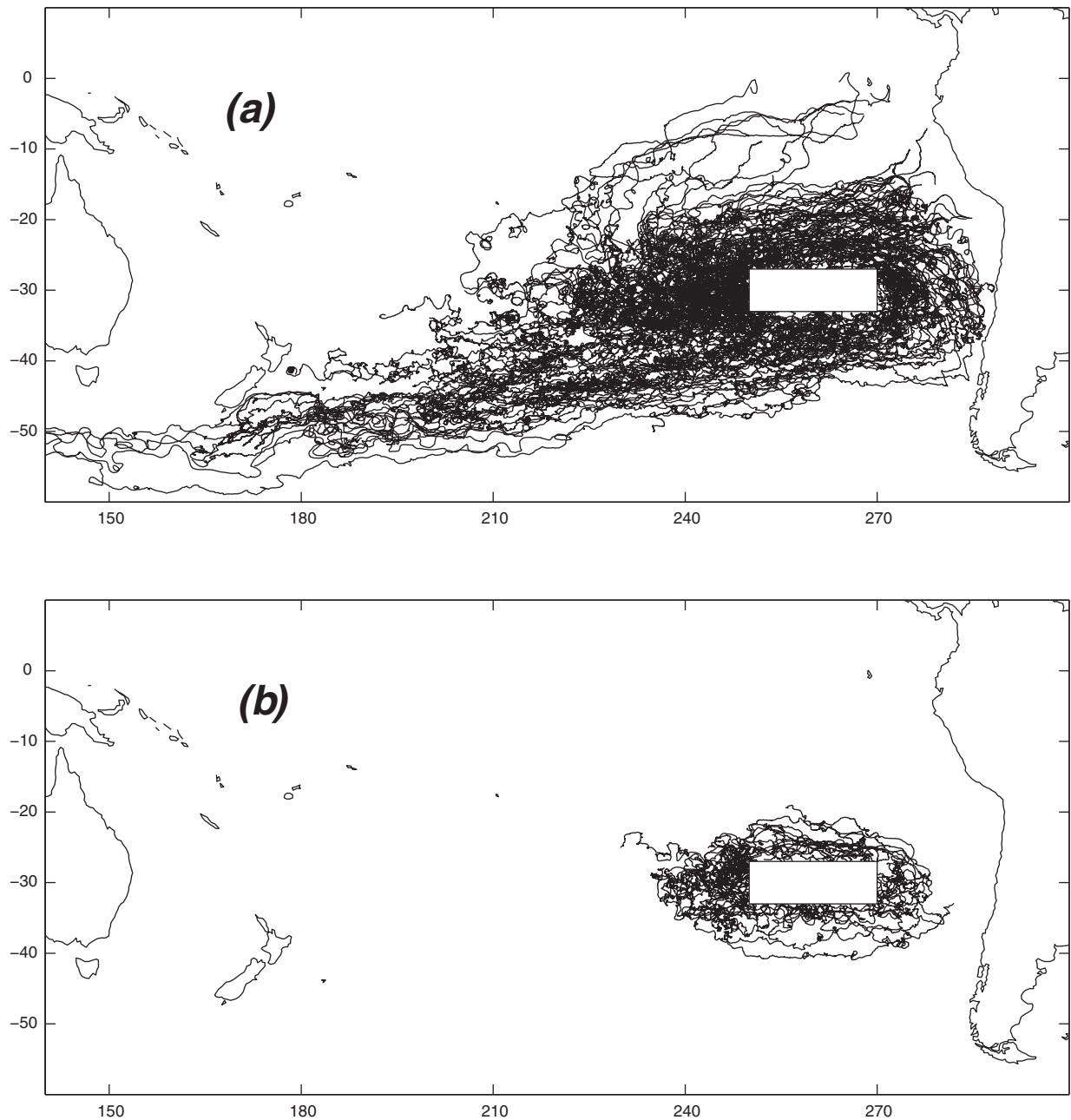
---

[4] www.5gyres.org

Fig. 6. Segments of trajectories of real drifters (a) before they entered and (b) after they left from area outlined with the rectangle, corresponding to the South Pacific zone of Fig. 4d.

(Law et al., 2010) clusters agree well with measurements of defragmented plastic, while observations in other oceans were missing until recently. As a result of collaborative effort, M. Eriksen[5] confirmed the South Indian patch in March–April 2010 and South Atlantic patch in September–December 2010,[6] and J. Mackey collected in January 2011 microplastic southeast of Easter Island, at locations close to the ones predicted by Fig. 4d and Table 1. Results have been presented at the 5th International Marine Debris Conference,[7] and corresponding publications are pending. While the accumulation zone in the South Pacific is the strongest in terms of the intensity

and steadiness of the convergence of surface currents, the observed concentration of debris there appears to be much lower than in the North Pacific. This can be explained by the fact that, while in Fig. 4 larger oceans receive more debris because of the homogeneous initial condition, in reality majority of plastic, originating from the land, has larger distances to travel. In addition, total consumption of plastic in the more economically developed Northern Hemisphere is expected to be higher.

A technique, developed as described in Appendix, suggests that the horizontal scale (e-folding rate) of the tracer density near a collection center $(R_c = (4\,k/|D|)^{1/2})$ is only a function of the flow convergence $|D|$ and diffusion k, and is not sensitive to boundary conditions or total amount of collected tracer. Details of locations, sizes, and shapes of the five strongest convergence zones, assessed with this technique, are gathered in

[5] www.5gyres.org
[6] http://www.newscientist.com/article/dn20295-pollutiontrawling-voyage-finds-oceans-plastic-soup.html
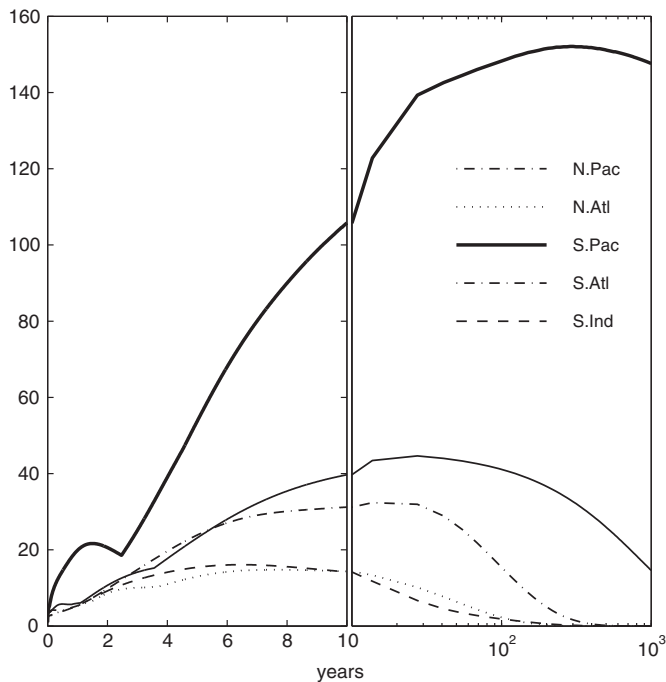[7] www.5imdc.org

Fig. 7. Changes in time of maximum values of the model drifter concentration in five subtropical gyres. At $t = 0$ concentration is constant and equal to the unity.

Table 1. In addition, at least three other, secondary collection zones were spotted in the model solution (e.g., Fig. 4c). Although these zones are relatively small in size and weak, and are dominated on long times by the stronger main zones, their vicinity to heavily populated coastal areas may make them important players in the actual debris distribution in the ocean. These secondary zones must be the ones discussed earlier by C. Ebbesmeyer.[8]

Because accumulation areas are associated with subtropical gyres, which are often viewed as basin-wide vortices, rotating anticyclonically, there is a popular misconception, suggesting that debris is trapped within these vortices because it circulates around their centers. The gyres are best seen in the dynamic topography [e.g., Maximenko and Niiler, 2005] whose isopleths are also streamlines of geostrophic flow (Fig. 9a). These streamlines are very different from the mean trajectories of drifters in Fig. 5a. Drifter motions are determined by a combination of geostrophic currents, controlled by the pressure gradient (i.e. by the sea level tilt), and effect of local wind. The latter effects include direct wind force applied to the surface float, Stokes drift by wind waves, and Ekman currents. Separation of these three components is difficult and Stokes drift may be as strong in the surface layer (Ardhuin et al., 2009) as Ekman currents (Ralph and Niiler, 1999). However, each component and their combination can be (at least roughly) approximated as simple functions to local wind or wind stress vectors. For simplicity, in this paper, we use the term "Ekman current" for the full current associated with the local wind. Mean streamlines of thus-defined Ekman currents, shown in Fig. 9b, are very different from geostrophic currents in Fig. 9a, and they form a large-scale pattern with five well defined convergent zones collocated with the drifter aggregation zones in Fig. 4d. Importantly, not every gyre collects debris, subpolar gyres do not. It is the convergence (divergence) of near-surface, wind-generated Ekman currents that (through the so-called Sverdrup mechanism) both induces the anticyclonic

(cyclonic) gyres and pushes floating objects towards subtropical gyres and away from subpolar gyres. Kubota et al. (2005) and Martinez et al. (2009) describe in details effects of geostrophic and Ekman currents on the motion of floating particles in their models of near-surface circulation in the North and South Pacific.

Different kinds of debris are known to move differently under same atmospheric and oceanic conditions. In many cases, the geometry of the floating object defines how the direct force from the wind combines with the effect of the upper-ocean currents, having complex vertical structure. This is well illustrated by the difference between motions of drifters, having a large drogue attached, and drifters that lost their drogues. Under the same current/wave/wind conditions, such drifters move quite differently (e.g., Kirwan et al., 1978, Maksimenko et al., 1993; Poulain et al., 2009). Even in the time-mean velocities, careful comparison between the panels of Fig. 10 reveals for undrogued drifters (b) systematically larger magnitudes and smaller angles to the wind than the same quantities for drifters, drogued at 15 m (a). However, despite of this difference, both drogued and undrogued drifters in Fig. 10 aggregate in the same areas on the long run. Locations of these convergences in the North Pacific[9] and North Atlantic (Law et al., 2010) also correspond to regions of observed high concentration of defragmented plastic. This suggests remarkable robustness of the pathways of marine debris that still needs to be explained.

The model used here is not free from shortcomings. Use of the finite (5 days) time step, which in some regions may be shorter than the local Lagrangian decorrelation time scale, allows the model pathways that were never taken by real drifters. A good example is crossing the equator (e.g., Fig. 8b). In reality, when such a crossing occurs, the drifters do not penetrate far, and they ultimately return to the original hemisphere. This artificial model effect is produced by temporal variability of currents combined with the too short model time step.

More generally, ocean currents are known to exhibit various modes of interannual and decadal variability, so that validity of the assumption of statistical stationarity can be questioned. The goal of the model, presented in this paper, is to provide a global view and simple general concept explaining the pattern and dynamics of the areas of marine debris aggregation in the World Ocean. More realism will be added to the analysis in future studies based on the surface velocity products, diagnosed using the satellite remote sensing, such as OSCAR[10] (Bonjean and Lagerloef, 2002) and SCUD[11] (Maximenko and Hafner, 2010). Similar models, used by Martinez et al. (2009) in the South Pacific, produced results identical to ours.

Convergences described in this paper are controlled by Ekman currents, having horizontal scale of atmospheric wind, far exceeding oceanic mesoscale. However, the details of the debris distribution on scales smaller than 100 km are often controlled by oceanic eddies and fronts. Fig. 4b and c illustrate this by revealing the elevated tracer concentration along the subtropical front north of Hawaii, marked by white dashed lines. Interaction between the large-scale supply of debris (Wilson et al., 2008) and its local redistribution (Calil and Richards, 2010) by mesoscale oceanic features is yet to be understood.

Acknowledgments

---

[8] www.oceanmotion.org

[9] http://www.algalita.org/research/plastic_pollution_GIS_maps.html
[10] http://www.oscar.noaa.gov/
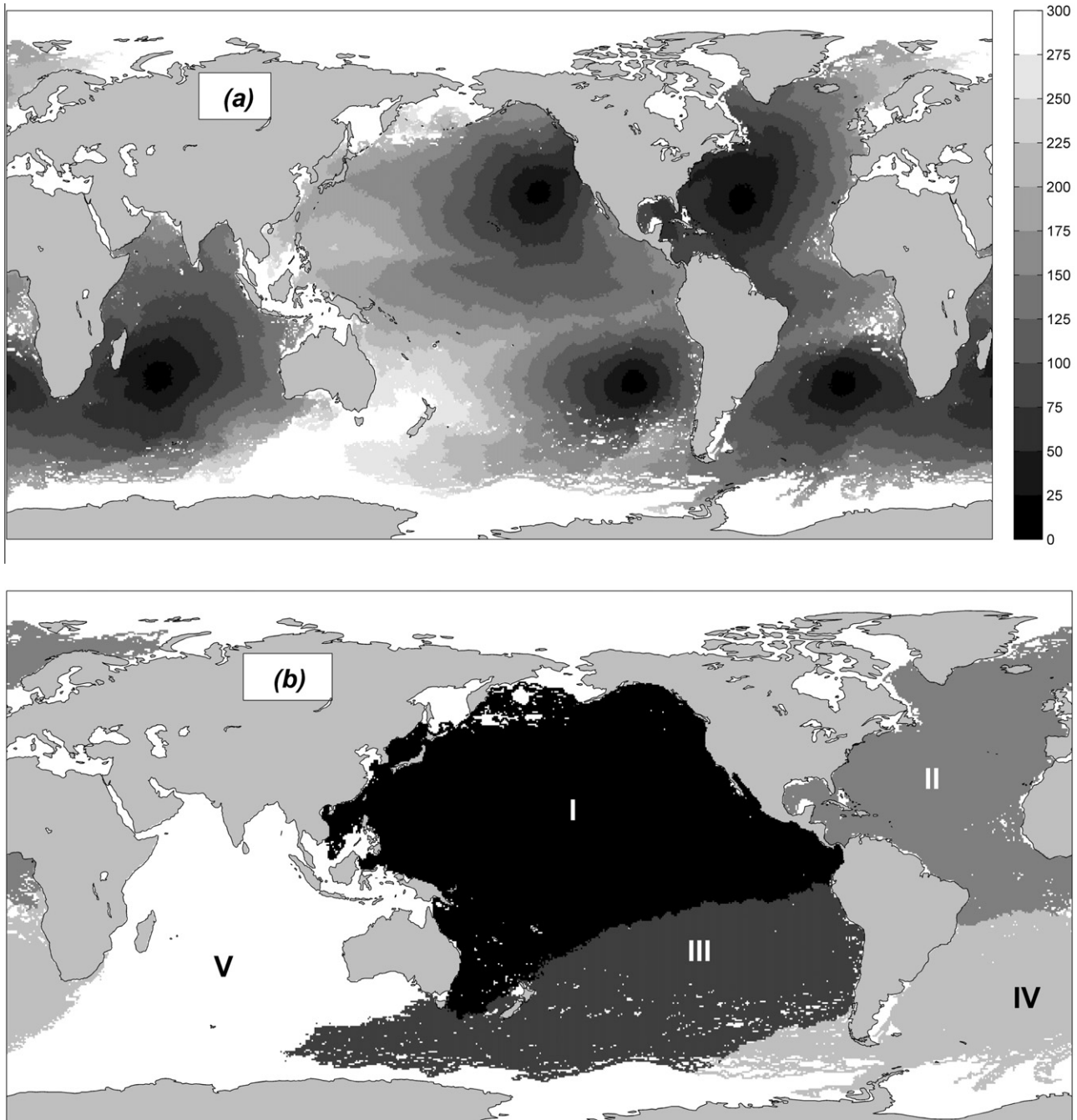[11] http://apdrc.soest.hawaii.edu/

Fig. 8. (a) Minimum time (days) required by model drifters, released at a given location, to reach one of the five collection centers, marked in Fig. 4d, and (b) index, showing which center is reached first.

Table 1
Locations, axes, and orientations of main subtropical collection areas.

Basin	Coordinates of the center[a]	Long axis R_{cx} (km)[b]	Short axis R_{cy} (km)[b]	Tilt (degree)[c]
North Pacific	31°N, 139°W	1220	800	+11.2
North Atlantic	29°N, 54°W	2120	814	+9.5
South Pacific	29°S, 99°W	1040	688	−7.1
South Atlantic	30°S, 13°W	1710	758	−8.7
South Indian	28°N, 62°E	2470	884	+3.3

[a] Centers (shown with dots in Fig. 4d) correspond to locations of the maxima of the model solution on year 10, additionally smoothed with the two-dimensional Hanning filter with the half-width of 1000 km.
[b] Axes are estimated from the isopleths of the model solution, shown in Fig. 4d, and indicate the e-fold decay scale in the corresponding direction.
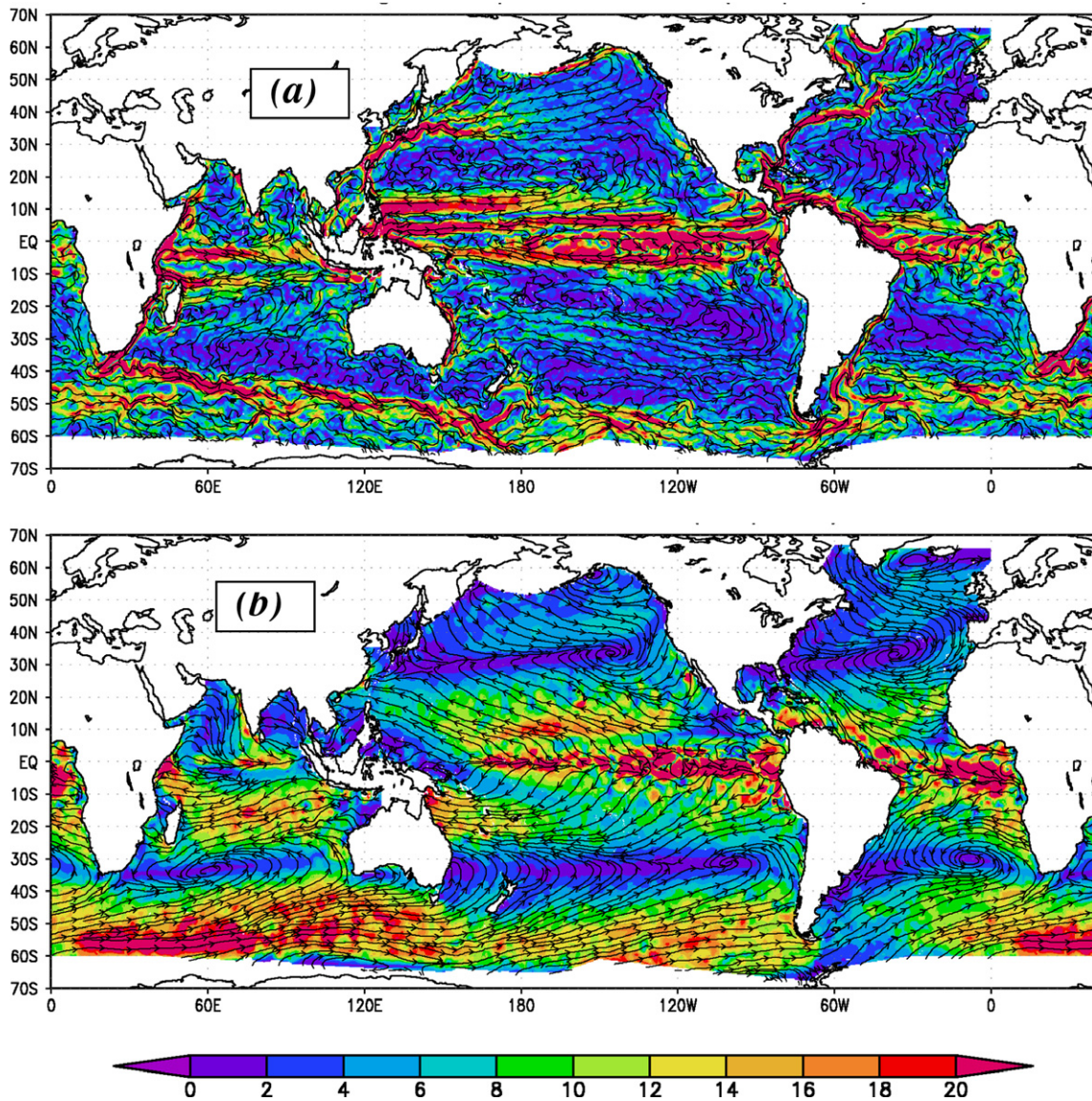[c] Angle (positive counterclockwise) between the long axis and the direction towards the east.

Fig. 9. Streamlines of (a) mean geostrophic currents and (b) mean Ekman currents from the SCUD data (Maximenko and Hafner, 2010). Colors indicate velocity magnitude and units are cm/s.

Appendix A. Stationary analytical solution of simplified tracer equation near the center of convergence

The equation for the passive tracer concentration C governed by horizontal advection and diffusion, is

$$\partial C / \partial t + \nabla (C \cdot \mathbf{V}) = \nabla (k \cdot \nabla C), \tag{A.1}$$

where $\partial / \partial t$ is time derivative, ∇ is operator of horizontal gradient, $\mathbf{V}$ is horizontal velocity vector, and k is mixing coefficient. Therefore, stationary solution satisfies

$$C \cdot \mathbf{V} = k \cdot \nabla C + \mathbf{F}, \tag{A.2}$$

where $\mathbf{F(r)}$ is an arbitrary vector field, such that $\nabla \cdot \mathbf{F} = 0$.

Let's consider axisymmetric currents (Fig. 11a) with velocity $\mathbf{V} = (D/2) \cdot \mathbf{r}$, D = const < 0, k = const, and boundary condition $C = C_0$ at $r = |\mathbf{r}| = R$. Divergence, $(\nabla \cdot \mathbf{V})$, of such velocity field is uniform in space and is equal to D. Assuming $\mathbf{F} = 0$, the solution of Eq. (A.2) is

$$C_a(r) = C_0 \cdot \exp\{D \cdot (r^2 - R^2)/(4k)\}. \tag{A.3}$$

Remarkably, C_a can be also presented as

$$C_a(r) = C_0 \cdot \exp\{(-D \cdot R^2)/(4k)\} \cdot \exp\{-(r/R_c)^2\}, \tag{A.4}$$

that suggests that the initial condition only affects the amplitude of the solution while the radius of the 'bell', $R_c = (4 k/|D|)^{1/2}$, is totally determined by the interplay between the velocity convergence and mixing. Stronger convergence and weaker mixing result into more compact areas of the tracer accumulation.

The role of $\mathbf{F}$ in more complex cases can be illustrated by adding (Fig. 11b) to the $\mathbf{V}$ axisymmetric azimuthal component $\mathbf{V_a} = (\mathbf{k} \times \mathbf{V})$, where $\mathbf{k}$ is the upward-looking unity vector and the cross denotes the vector product. Easy to see that $\mathbf{V_a}$ corresponds to clockwise solid rotation at angular speed $D/2$. As streamlines of
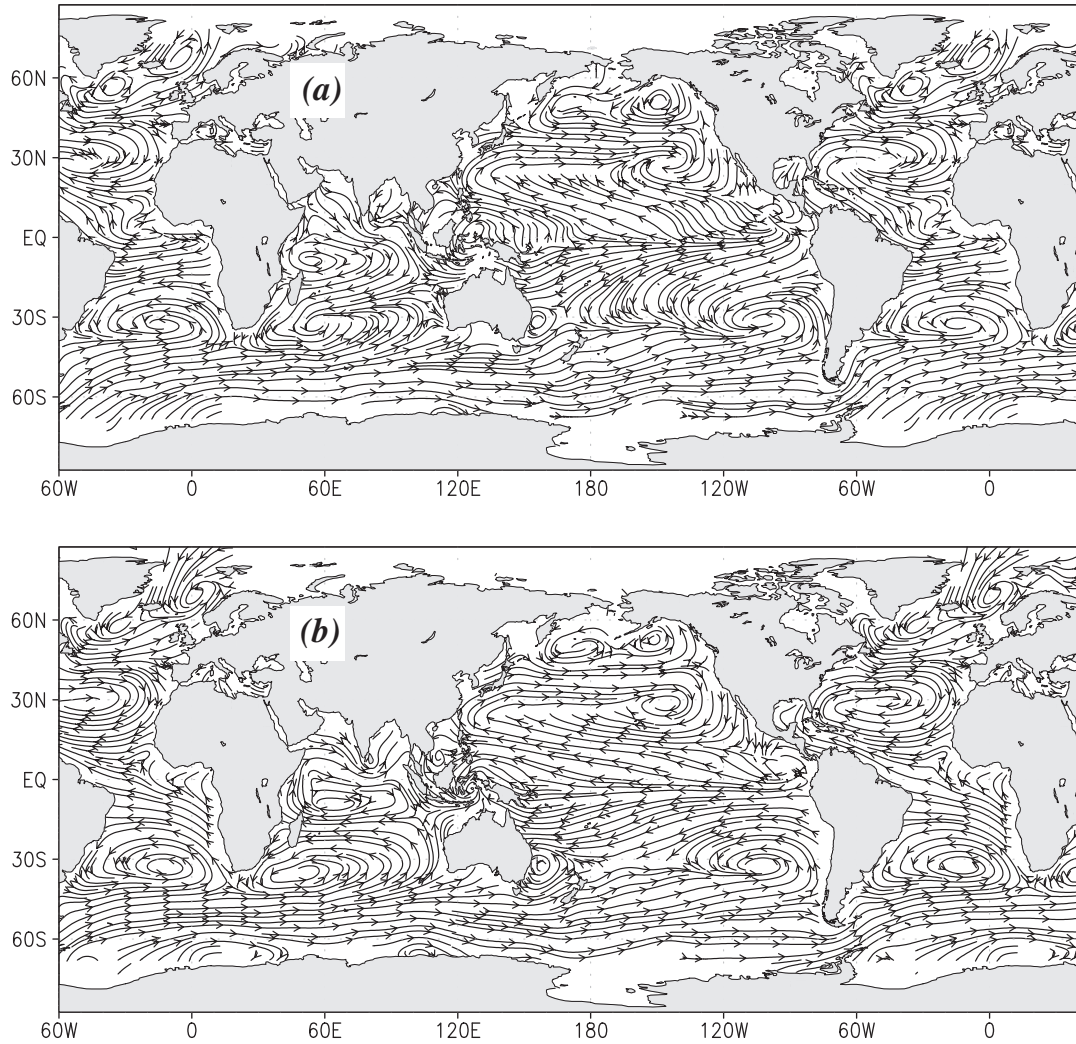
Fig. 10. Ensemble-mean streamlines, derived from trajectories of drogued (a) and undrogured (b) drifters. (Streamlines are smoothed for clarity of presentation.)
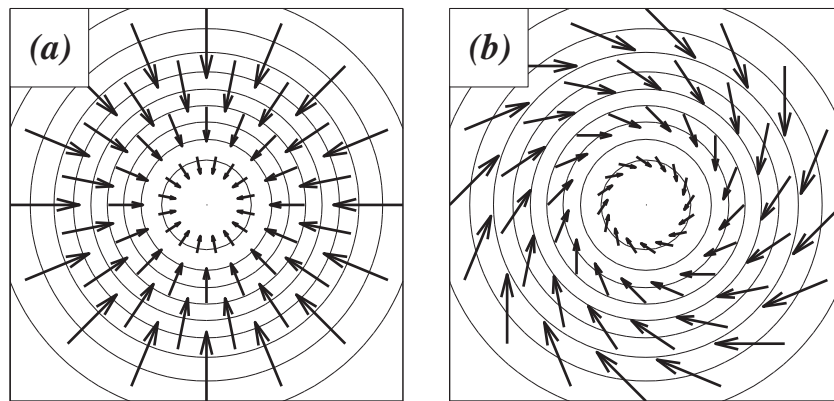

Fig. 11. Velocity vectors and contours of concentration for the solution of tasks (a) without and (b) with the azimuthal rotation added.

$\mathbf{V_a}$ are parallel to isopleths of C_a and $\nabla \cdot \mathbf{V_a} = \mathbf{0}$, it would have no effect on the solution of the original Eq. (A.1). However, in Eq.(A.2) it would produce the advective flux ($C_a \cdot \mathbf{V_a}$) that would be perpendicular to the diffusive flux $k\nabla \cdot C_a$, and therefore could not be balanced by the mixing term. Thus, in Eq. (A.2) $\mathbf{F}$ compensates for the effect of advection by the solenoidal component of velocity.

Note that in the absence of the solenoidal component, velocity $\mathbf{V}$ can be described using the 'potential' P.

$$\mathbf{V} = \nabla P, P = D \cdot r^2/4. \tag{A.5}$$

This allows some generalization of the solution for anisotropic (elliptical) case. Easy to see that solution of Eq. (A.2) with $\mathbf{F} = 0$, $k = $ const, $P = P_0 \cdot \{(x/R_x)^2 + (y/R_y)^2\}$ $(P_0 = D/2 \cdot R_X^2 \cdot R_Y^2/(R_X^2 + R_Y^2) < 0$ for converging currents), and boundary condition of $C = C_0$ at $(x/R_x)^2 + (y/R_y)^2 = n^2$, is

$$C_e(\mathbf{r}) = C_0 \cdot \exp\{P_0/k \cdot ((x/R_x)^2 + (y/R_y)^2 - n^2)\}. \tag{A.6}$$

N. Maximenko et al. / Marine Pollution Bulletin 65 (2012) 51–62

This solution can also be rewritten as

$$C_e(\mathbf{r}) = C_0 \cdot \exp\{-P_0 \cdot n^2/k\} \cdot \exp\{-(x/R_{cx})^2 - (y/R_{cy})^2)\}, \qquad (A.7)$$

so that the influence of the initial condition is limited to the amplitude of C_e. The isopleths of C_e are ellipses with the axes R_{cx} and R_{cy} totally defined by convergence and mixing and independent from the initial condition:

$$R_{cx} = (2k/|D| \cdot (1 + (R_x/R_y)^2)^{1/2},$$
$$R_{cy} = (2k/|D| \cdot (1 + (R_y/R_x)^2))^{1/2}. \qquad (A.8)$$

Values of R_{cx} and R_{cy} and orientation of the principal axes for the five subtropical collection zones, estimated from the solution of the statistical model, shown in Fig. 4d, are summarized in Table 1.

References

Ardhuin, F., Marié, L., Rascle, N., Forget, P., Roland, A., 2009. Observation and estimation of Lagrangian, Stokes, and Eulerian currents induced by wind and waves at the sea surface. J. Phys. Oceanogr. 39, 2820–2838.

Bonjean, F., Lagerloef, G.S.E., 2002. Diagnostic model and analysis of the surface currents in the tropical pacific ocean. J. Phys. Oceanogr. 32, 2938–2954.

Calil, P.H.R., Richards, K.J., 2010. Transient upwelling hot spots in the oligotrophic North Pacific. J. Geophys. Res. 115, C02003. doi:10.1029/2009JC005360.

Dohan, K., Maximenko, N., 2010. Monitoring ocean currents with satellite sensors. J. Oceanogr. 23 (4), 94–103.

Hansen, D.V., Poulain, P.-M., 1996. Quality control and interpolations of WOCE/TOGA drifter data. J. Atmos. Oceanic Technol. 13, 900–909.

Kershaw, P., Katsuhiko, S., Lee, S., Samseth, J., Woodring, D., 2011. Plastic Debris in the Ocean. United Nations Environmental Programme Year Book 2011, pp. 20–33.

Kirwan Jr., A.D., McNally, G., Pazan, S., 1978. Wind drag and relative separations of undrogued drifters. J. Phys. Oceanogr. 8, 1146–1150.

Kubota, M., 1994. A mechanism of the accumulation of floating marine debris north of Hawaii. J. Phys. Oceanogr. 24, 1059–1064.

Kubota, M., Takayama, K., Namimoto, D., 2005. Pleading for the use of biodegradable polymers in favor of marine environments and to avoid an asbestos-like problem for the future. Appl. Microbiol. Biotechnol. 67, 469–476. doi:10.1007/s00253-004-1857-2.

Law, K.L., Morét-Ferguson, S., Maximenko, N.A., Proskurowski, G., Peacock, E.E., Hafner, J., Reddy, C.M., 2010. Plastic accumulation in the North Atlantic Subtropical Gyre. Science 329, 1185–1188.

Lumpkin, R., Treguier, A.-M., Speer, K., 2002. Lagrangian Eddy scales in the Northern Atlantic Ocean. J. Phys. Oceanogr. 32, 2425–2440.

Maksimenko, N.A., Niiler, P.P., Sybrandy, A.L., Kharlamov, A.I., 1993. Drifter experiment in Black Sea. Oceanology 33 (3), 379–383 (English translation).

Martinez, E., Maamaatuaiahutapu, K., Taillandier, V., 2009. Floating marine debris surface drift: convergence and accumulation toward the South Pacific subtropical gyre. Mar. Pollut. Bull. 58, 1347–1355.

Maximenko, N.A., Niiler, P.P., 2005. Hybrid decade-mean global sea level with mesoscale resolution. In: Saxena, N. (Ed.), Recent Advances in Marine Science and Technology 2004. PACON International, Honolulu, pp. 55–59.

Maximenko, N., Niiler, P., Rio, M.-H., Melnichenko, O., Centurioni, L., Chambers, D., Zlotnicki, V., Galperin, B., 2009. Mean dynamic topography of the ocean derived from satellite and drifting buoy data using three different techniques. J. Atmos. Oceanic Technol. 26, 1910–1919.

Maximenko, N., Hafner, J., 2010. SCUD: Surface CUrrents from Diagnostic Model. IPRC Technical Note No. 5, February 16, 2010, 17p.

Meehl, G.A., 1982. Characteristics of surface current flow inferred from a global ocean current dataset. J. Phys. Oceanogr. 12, 538–555.

Moore, C., Moore, S.L., Leecaster, M.K., Weisberg, S.B., 2001. A comparison of plastic and plankton in the north pacific central gyre. Mar. Pollut. Bull. 42(12), 1297–1300, 2001-12-01. doi:10.1016/S0025-326X(01)00114-X.

Niiler, P.P., 2001. In: Siedler, G., Church, J., Gould, J. (Eds.), The World Ocean Surface Circulation. Academic Press, pp. 193–204.

Niiler, P.P., Davis R.E., et al., 1987. Water-following characteristics of a mixed layer drifter. Deep-Sea Res. Part A – Oceanogr. Res. Papers 34(11), 1867–1881.

Niiler, P.P., Paduan, J.D., 1995. Wind-driven motions in the Northeast Pacific as measured by Lagrangian drifters. J. Phys. Oceanogr. 25 (11), 2819–2830.

Poulain, P.-M., Gerin, R., Mauri, E., Pennel, R., 2009. Wind effects on drogued and undrogued drifters in the eastern Mediterranean. J. Atmos. Oceanic Technol. 26, 1144–1156.

Ralph, E.A., Niiler, P.P., 1999. Wind-driven currents in the tropical Pacific. J. Phys. Oceanogr. 29, 2121–2129.

Sybrandy, A.L., Niiler, P.P., 1991. WOCE/TOGA Lagrangian Drifter Construction Manual. WOCE Rep. 63, SOI Ref. 91/6. Scripps Inst. of Oceanogr., La Jolla, Calif, 58pp.

Wakata, Y., Sugimori, Y., 1990. Lagrangian motions and global density distribution of floating matter in the ocean simulated using shipdrift data. J. Phys. Oceanogr. 20, 125–138.

Wilson, C., Villareal, T.A., Maximenko, N., Bograd, S.J., Montoya, J.P., Schoenbaechler, C.A., 2008. Biological and physical forcings of late summer chlorophyll blooms at 30 N in the oligotrophic Pacific. J. Mar. Syst. 69, 164–176.